Science Advances

AAAS

advances.sciencemag.org/cgi/content/full/4/3/eaao3757/DC1

Supplementary Materials for

Variations in the amount of water ice on Ceres' surface suggest a seasonal water cycle

Andrea Raponi, Maria Cristina De Sanctis, Alessandro Frigeri, Eleonora Ammannito, Mauro Ciarniello, Michelangelo Formisano, Jean-Philippe Combe, Gianfranco Magni, Federico Tosi, Filippo Giacomo Carrozzo, Sergio Fonte, Marco Giardino, Steven P. Joy, Carol A. Polanskey, Marc D. Rayman, Fabrizio Capaccioni, Maria Teresa Capria, Andrea Longobardo, Ernesto Palomba, Francesca Zambon, Carol A. Raymond, Christopher T. Russell

Published 14 March 2018, *Sci. Adv.* **4**, eaao3757 (2018)
DOI: 10.1126/sciadv.aao3757

This PDF file includes:

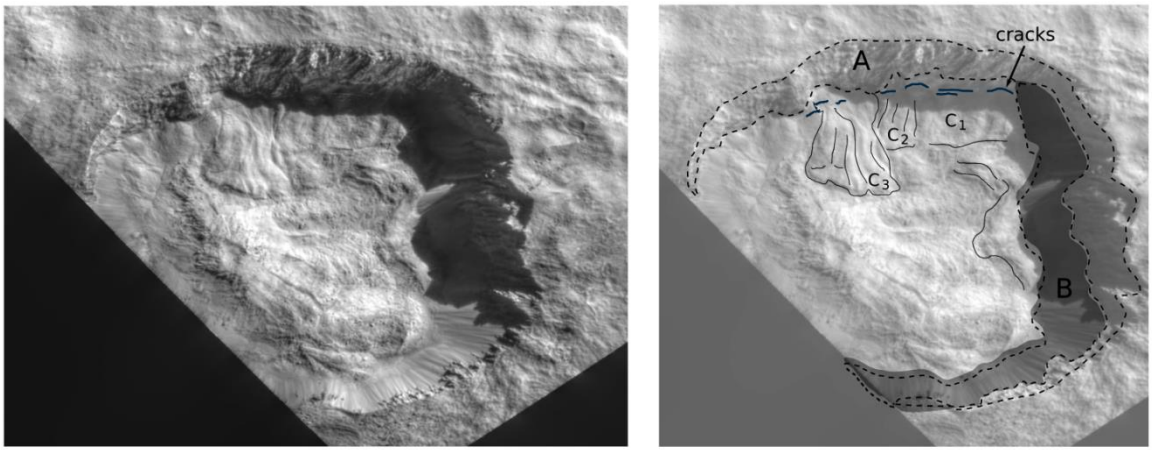

fig. S1. **Geological context.** Left panel: FC image taken at L1. The shadowed regions have been enhanced. Right panel: Main geomorphologic features. A: sub-vertical scarp. B: crater wall's loose deposits. C1, C2, C3: lobate deposits with longitudinal furrows and fan-like shapes, similar to Earth's flowing rock-glacier. These glaciers are fed by material that accumulates at the base of the vertical scarp (**A**), three consecutive deposition events can be recognized (1,2,3), with C3 being the youngest. Within the shadowed areas of the northern walls, a series of clear iso-oriented opened cracks are present. The cracks are 1 to 1.5 km long and oriented parallel to the crater wall, along the base of the northern wall. The absence of impact craters in both the walls and the floor, and the shape of the crater indicate that mass wasting processes have been actively reshaping the crater.

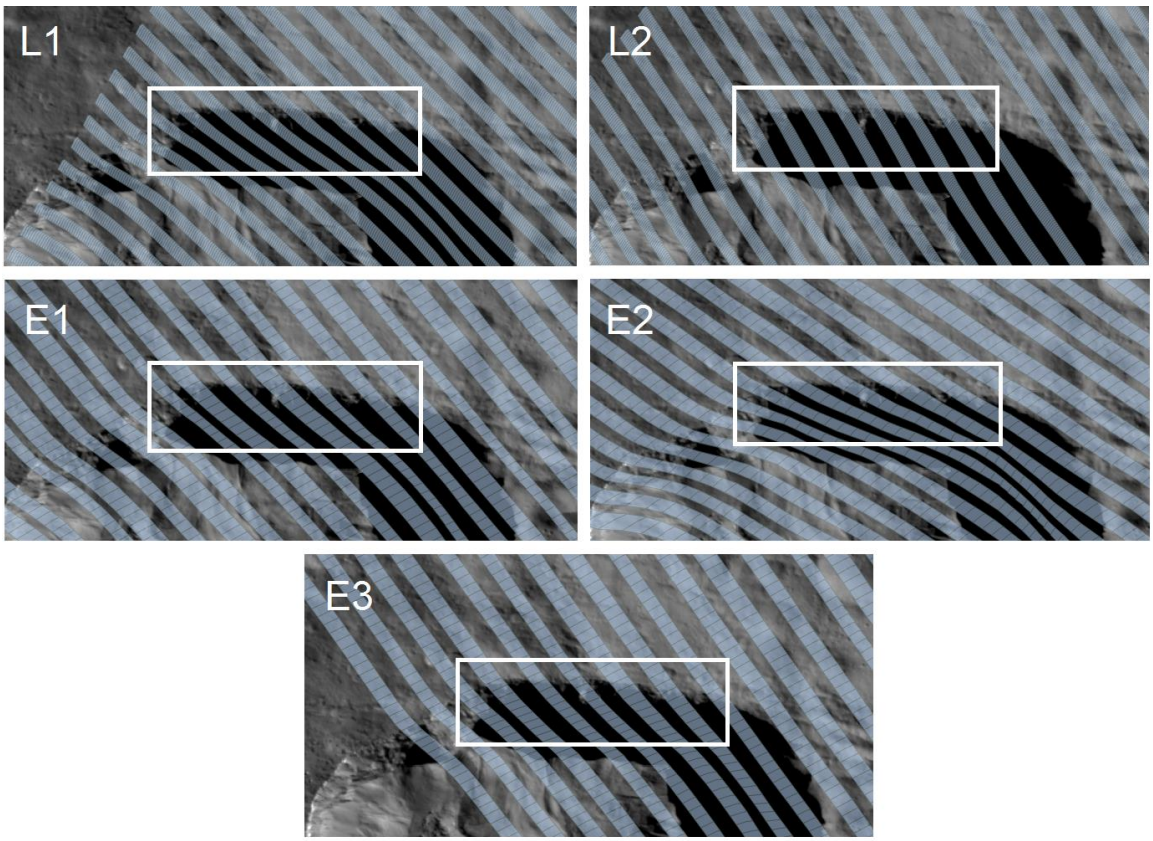

fig. S2. **Footprints of the VIR data visualized over the Framing Camera image mosaic.** Each blue stripe represents a slit which is divided into 'pixels'. Every pixel's footprint corresponds to a single spectrum. Pixels inside the white rectangles are averaged to produce the observed spectra (shown in Fig. 2). Number of pixels considered is specified in table S1.

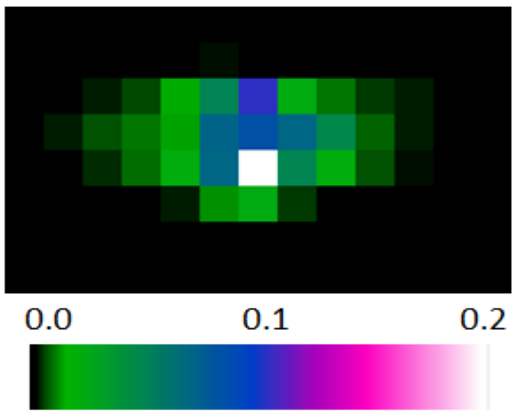

fig. S3. **Point spread function of the VIR instrument as derived from star observations.** The total flux is normalized to 1, thus each pixel receives a fraction of the flux of a point source as indicated by its color. The axes correspond to the spatial dimensions: the x-axis is in the slit direction; the y-axis is in the scan direction. The value of each pixel is the median over the spectral range considered in the present work (1.15-3.55 μm).

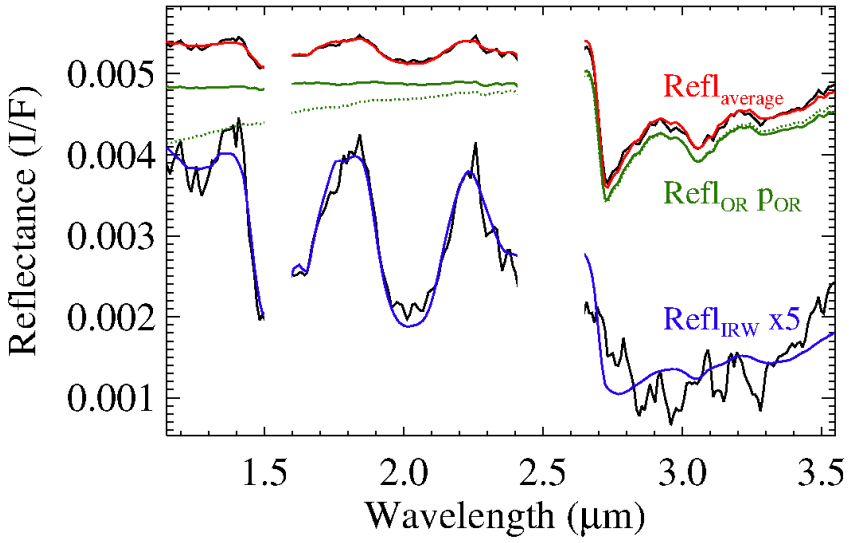

fig. S4. **Model of the average spectrum as a sum of outer region signal and ice-rich wall signal.** L1 observation, from the top: $Refl_{average}$ = average spectrum (black), and the modeled best fit (red); $Refl_{OR} \cdot p_{OR}$ = modeled reflectance of outer regions multiplied by its relative contribution to the total signal, with (green solid line) and without (green dotted line) the correction factor ***f*** discussed in Materials and Methods; $Refl_{IRW}$ (reflectance of shadowed ice-rich wall) = $Refl_{average} - Refl_{OR}\, p_{OR}$, of both measured spectrum (black) and model (blue). Here it is multiplied by a factor of 5 for the sake of clarity.

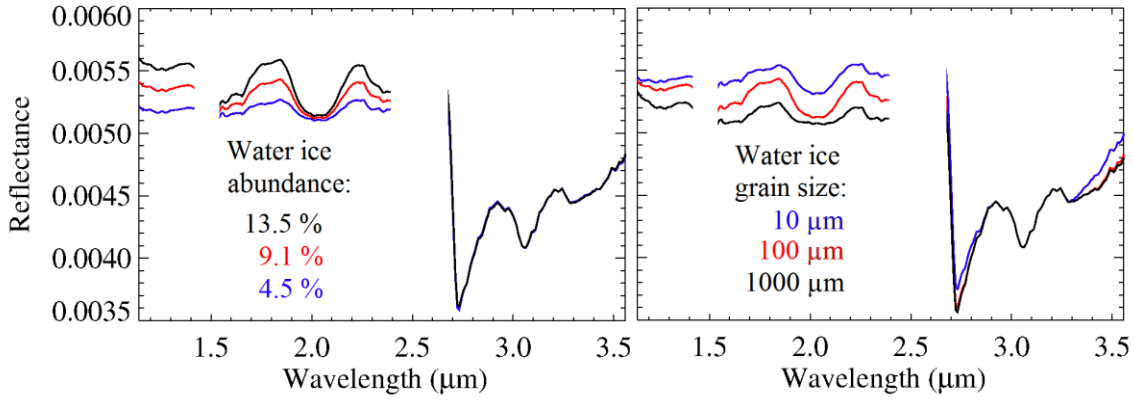

fig. S5. Modeled spectra with different abundances (left) and grain size (right). In both panels red spectrum corresponds to the best fit of L1 observation, modeled as described in the supplementary methods. Retrieved values of water ice properties for L1 are 9.1% in abundance, and 100 μm in grain size. Differences between L1 and E1 observations shown in Fig. 3 (higher signal level in the 1.1 – 2.5 μm range, and larger band area at 2.0 μm in E1) are consistent with increased water ice abundance (see left panel). Conversely, a variation of grain size is not compatible with the measured spectra (see right panel).

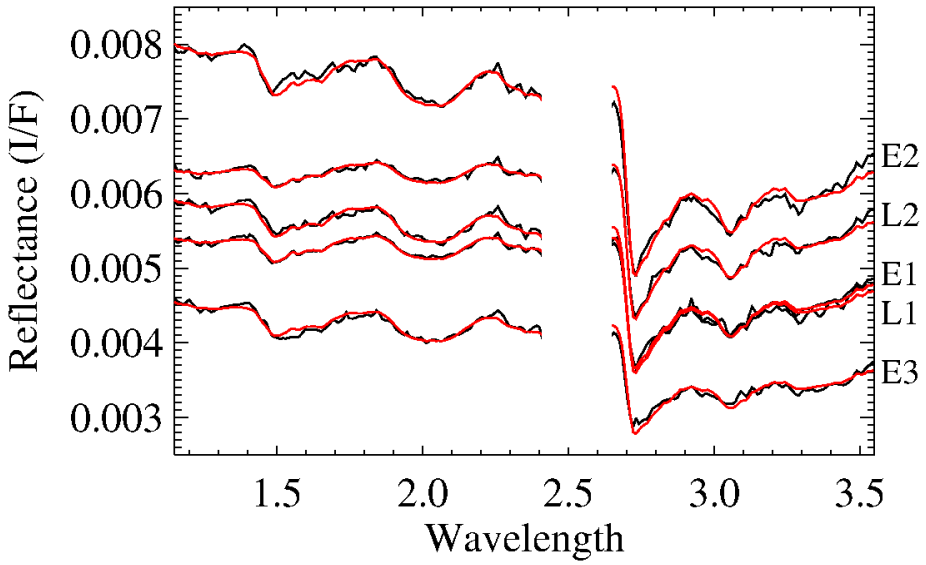

fig. S6. **Modeled best fits (red lines) of the 5 average spectra (black lines).** Models (red lines) are obtained as described in Materials and Methods.

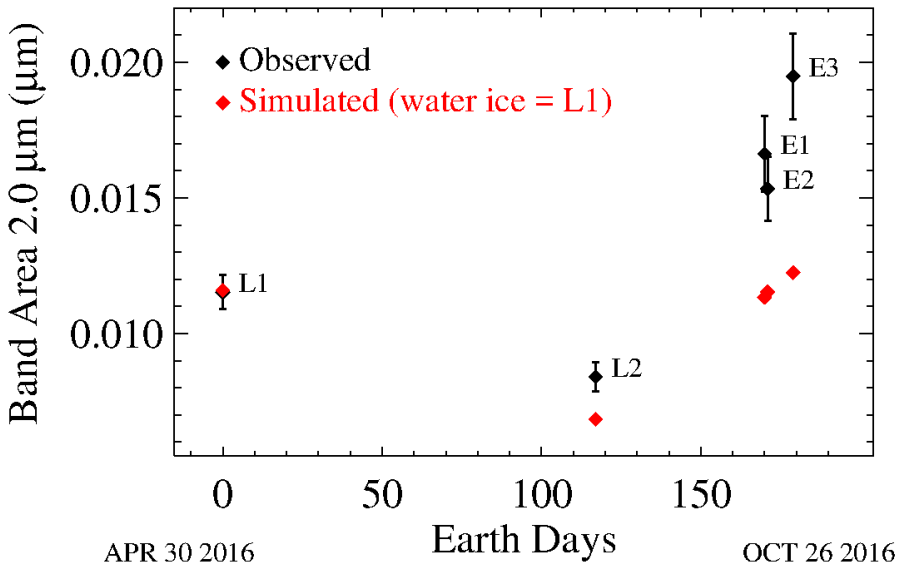

fig. S7. **Model assuming constant water ice.** Black diamonds: measured band area of the average spectrum of the 5 observations as a function of Earth days (as in Fig 2). Red diamonds: simulated band area by assuming a constant water ice abundance as retrieved in L1 (p_{WI}), but keeping the information on the viewing geometry for each observation (p_{IRW}). These parameters (Table S2) are used in Eqs. 1-3 (Spectral Modeling section) to simulate the spectra, and thus to derive the band area plotted here.

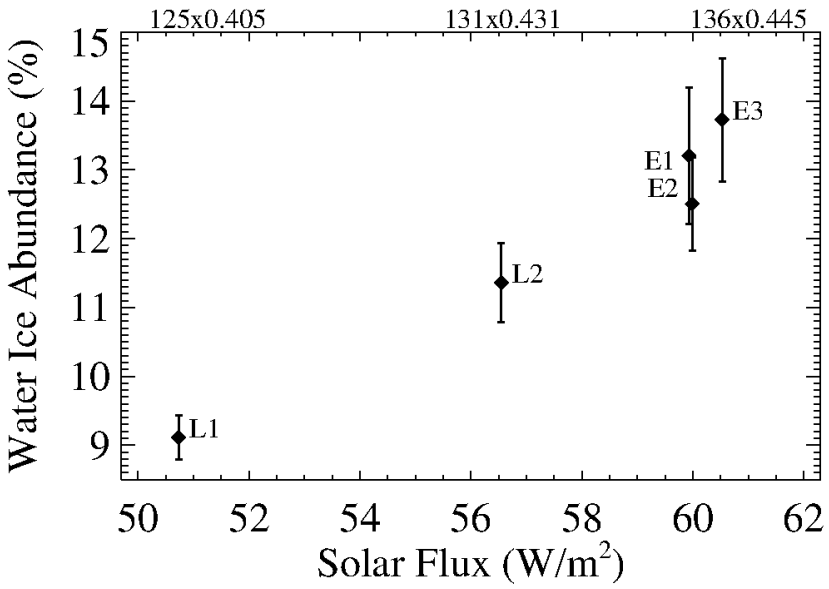

fig. S8. **Water ice abundance of the ice-rich wall as a function of average solar flux.** Solar flux is calculated at noon in the floor area adjacent to the ice-rich wall in correspondence with the rock glaciers (10 x 5 km^2). The average solar flux increases because of decreasing incidence angle, heliocentric distance, and shadowed area. The upper axis shows the solar flux multiplied by the fraction of the illuminated area, which gives as a result the average flux (lower axis). The clear correlation points to a relation between the increase in water abundance and the intensification of the heat flux on the crater.

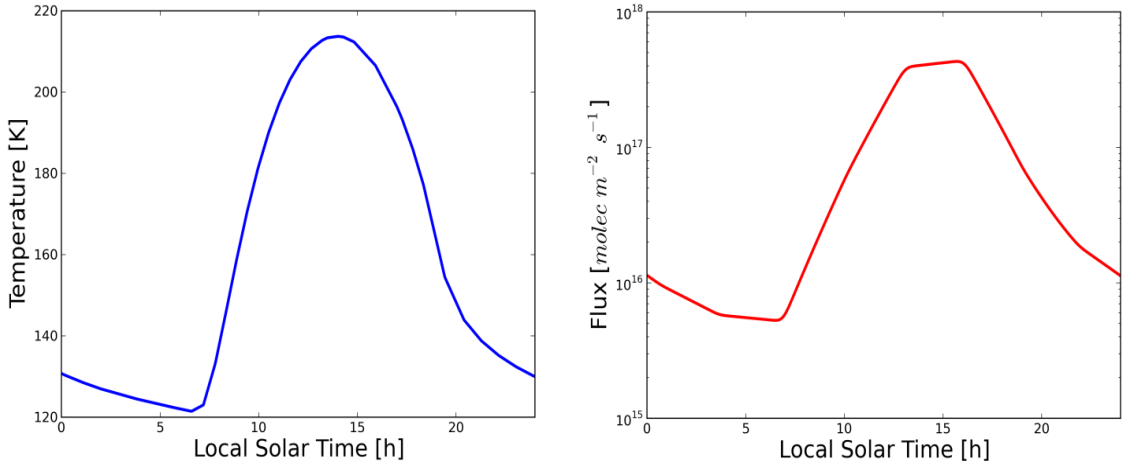

fig. S9. Water vapor flux modeled. Left panel: modeled average temperature of Juling's crater floor as a function of the local solar time, in correspondence with the Herschel observation on 24 October 2012. Right panel: modeled vapor flux, assuming water ice under a 1-cm regolith layer. The modeled water flux over the total crater floor surface (~3x10^8 m^2) results as compatible with the value derived by the Herschel observation (~10^{26} molec/s) (*11*). However, the subsurface ice can be deeper producing a lower amount of vapor flux.

table S1. **Viewing geometry of the five observations.** The column indicates respectively: labels used in the text; SpaceCraft Event Time of the observation; Number of pixels in the target area; incidence (i), emission (e), and phase (p) angles of the region outside the crater (but within the target area); Local Solar Time; Heliocentric Distance (au); Start observation time (UTC). The ice-rich wall is always in shadow. Uncertainties indicate the standard deviation within the region of interest.

label	SCET	N px	i ±1°	e ±1°	p ±0.5°	LST (h)	HD (au)	Observation Time (Start)
L1	515301741	341	53.8	18.6	70.3	9.40	2.961	2016-04-30 15:21:12.434
L2	525396659	297	61.1	10.6	54.3	8.58	2.913	2016-08-25 11:29:50.341
E1	529971002	71	54.5	16.9	69.1	9.19	2.881	2016-10-17 10:08:53.117
E2	530038462	73	41.7	35.8	71.2	10.72	2.881	2016-10-18 04:53:13.114
E3	530721999	71	60.7	22.0	73.6	8.56	2.876	2016-10-26 02:45:29.592

table S2. **Parameters and their errors retrieved in the best-fitting procedures as described in Materials and Methods.** $\mathbf{p_{WI}}$ is the fraction of the total cross section of icy grains, over the total area of the ice-rich wall. We refer to this parameter as the "water ice abundance" in the text. $\mathbf{p_{IRW}}$ is the cross section of the ice-rich wall as a fraction of the total projected area of interest (white rectangles in fig. S2).

label	Measured Band Area 2.0 μm (μm)	Ice-rich wall Band Area 2.0 μm (μm)	$p_{WI} \pm \sigma$ (%)	$p_{IRW} \pm \sigma$ (%)
L1	0.01152 ± 0.00063	0.1130 ± 0.0017	9.11 ± 0.32	69.1 ± 1.2
L2	0.00840 ± 0.00054	0.1234 ± 0.0023	11.36 ± 0.57	62.6 ± 1.4
E1	0.01648 ± 0.00140	0.1301 ± 0.0033	13.21 ± 0.99	68.8 ± 1.9
E2	0.01546 ± 0.00118	0.1277 ± 0.0025	12.50 ± 0.68	67.7 ± 1.8
E3	0.01948 ± 0.00157	0.1318 ± 0.0028	13.73 ± 0.89	71.7 ± 2.1